GSA Data Repository 2019404

Yang, K., Fan, H., Pirajno, F., and Li, X., 2019, The Bayan Obo (China) giant REE accumulation conundrum elucidated by intense magmatic differentiation of carbonatite: Geology, v. 47, ttps://doi.org/10.1130/G46674.1

Data Repository File: Text

Analytical methods

1. Mineragraphy

Cathodoluminescence (CL) microscopy was carried out on a Reliotron III stage with an electron beam in a moderately-high vacuum at Institute of Geology and Geophysics, Chinese Academy of Sciences (IGGCAS). Backscattered electron (BSE) image and energy dispersive x-ray spectroscopy (EDS) elemental mapping were carried out on a Nova NanoSEM 450 field emission scanning electron microscope (FESEM) at IGGCAS.

2. Apatite, dolomite and calcite LA-ICPMS trace elements

Trace element analyses for apatite were performed in a LA-ICPMS apparatus at the State Key Laboratory of Geological Processes and Mineral Resources, China University of Geosciences (Wuhan). Detailed operating conditions for LA system and ICP-MS can be found in Liu et al. (2008). Laser sampling was performed on a Geolas 2005. Ion-signal intensities were acquired through an Agilent 7500a ICP-MS instrument with helium (He) as the carrier gas and argon (Ar) as make-up gas. He and Ar were mixed via a T-connector before entering the ICP. Nitrogen (N_2) was added into the central He-Ar gas flow of the Ar plasma, in order to lower the detection limit and improve precision (Hu et al., 2008). Spot size of 44 μm was chosen in this study. Each analysis incorporated a background acquisition for approximately 20-30 seconds followed by 50 seconds of data acquisition.

Trace element analyses for dolomite and calcite were performed in a LA-ICPMS apparatus at State Key Laboratory of Ore Deposit Geochemistry, Institute of Geochemistry, Chinese Academy of Sciences. The detailed analytical procedures were similar to Chen et al. (2011). Laser sampling was performed using a GeolasPro 193nm wavelength ArF excimer laser ablation system, which was connected to an Agilent 7900 ICP-MS instrument. Helium (He) was used as the carrier gas and argon (Ar) as make-up gas mixed via a T-connector before entering the ICP. Each analysis incorporates an approximately 20-30 seconds background acquisition followed by 50 seconds data acquisition from the sample. Every eight spot was followed by one analysis of NIST SRM 610 in order to correct the time-dependent drift of sensitivity and mass discrimination of ICP-MS (Liu et al., 2008).

3. Apatite SIMS O isotopes

In situ oxygen isotope of apatite was measured using the Cameca IMS 1280 SIMS at IGGCAS, and the analytical procedures are the same as zircon above. The IMF is corrected using Durango apatite as a reference with a $\delta^{18}O$ value of 9.45‰ (Trotter et al., 2008). Qinghu apatite was used in this analysis as external reference, with $\delta^{18}O$ value of 5.20‰. The internal precision of $^{18}O/^{16}O$ ratios is ca. 0.2‰ (2σ). The external reproducibility of $^{18}O/^{16}O$ ratios by repeated measurements of standard is better than 0.40‰. The Durango and Qinghu apatite were also analyzed with the apatite samples as reference and yielded an average$\delta^{18}O$ values of 9.42‰ and 5.10‰, respectively, which are consistent with the standard values.

4. Apatite LA-MC-ICPMS Sr-Nd isotopes

Nd isotope measurements were carried out on a Thermo-Finnigan Neptune MC-ICPMS, coupled with 193 nm ArF Excimer laser ablation system, at IGGCAS. The detailed analytical procedures followed those in Yang et al. (2008). The energy density used in this study was set at 15 J/cm^2, and the laser spot size was 90 μm with pulse rate of 6 Hz. The aerosol ablated by the laser was transported to the mass spectrometer for isotopic determination using He as the carrier gas. Each spot analysis consisted of approximately 60 s data acquisition. Every 5 sample analyses were followed by one AP2 apatite reference measurement for external calibration, with standard $^{143}Nd/^{144}Nd$ value of 0.511007 ± 3 (Yang et al., 2014).

Sr isotopic composition was measured directly by MC-ICPMS at IGGCAS, due to the high concentration of these isotopes in apatite (Bizzarro et al., 2003; Waight et al., 2002). Yang et al. (2009) developed an in situ Sr determination method on a Thermo-Finnigan Nepture MC-ICPMS coupled with 193 nm ArF Excimer laser ablation system. The laser energy is set at 80 mJ, with energy density of 15 J/cm^2. In this analysis, the spot size was chosen as 44 μm with pulse rate of 8 Hz. The aerosol ablated by the laser was transported to the mass spectrometer for isotopic determination using He as the carrier gas. AP1 apatite was applied here as external reference material, with $^{87}Sr/^{86}Sr$ value of 0.711370 ± 7 (Yang et al., 2014). Every 10 sample analyses were followed by one AP1 apatite reference measurement for external calibration.

5. Monazite LA-ICPMS Th-Pb dating

Th-Pb isotopic dating of monazite were determined using Agilent Q-ICPMS, equipped with a 193 nm laser-ablation system at IGGCAS. The laser ablation spot size is 24μm. For detailed operating conditions and procedures monazite dating, please refer to Liu et al. (2008) and Xie et al. (2008). Monazite 44069 and 554 were selected as external and monitor standards for monazite Th-Pb dating. The corresponding reference ages for these two standard are 424.9 ±0.5 Ma for 44069 (ID-TIMS U-Pb, Aleinikoff et al., 2006) and 45.3 ± 1.4 Ma for 554 (ID-TIMS Th-Pb, Harrison et al., 1999). The $^{208}Pb/^{232}Th$ ratios were calculated by GLITTER program (Griffin et al., 2008). Weighted mean ages were calculated and plotted by Isoplot (v3) (Ludwig, 2003).

6. Whole rock Sr and Nd isotope

Whole rock Sr and Nd isotopes were analyzed at IGGCAS. Whole rock powders (100 mg) were dissolved in Teflon bombs after being spiked with ^{87}Rb, ^{84}Sr, ^{149}Sm and ^{150}Nd tracers prior to $HF+HNO_3+HClO_4$ dissolution. Rb, Sr, Sm and Nd were separated using conventional ion exchange procedures and measured using a Finnigan MAT262 multi-collector mass spectrometer. Detailed analytical procedures and isotope ratio measurements followed those given in Chen et al. (2000). The total procedural blanks for Rb-Sr and Sm-Nd were less than 100 pg and 50 pg, respectively. Precision of the concentrations is within 0.5 % of the quoted values (2σ). Data regression of isochron age calculation were performed with the ISOPLOT ver. 3.0 software (Ludwig, 2003).

References for Data Repository

Aleinikoff, J.N., Schenck, W.S., Plank, M.O., Srogi, L., Fanning, C.M., Kamo, S.L., and Bosbyshell, H., 2006, Deciphering igneous and metamorphic events in high-grade rocks of the Wilmington Complex, Delaware: morphology, cathodoluminescence and backscattered electron zoning, and SHRIMP U-Pb geochronology of zircon and monazite: Geological Society of America Bulletin, v. 118, p. 39–64, https://doi.org/10.1130/B25659.1.

Bizzarro, M., Simonetti, A., Stevenson, R., and Kurszlaukis, S., 2003, In situ $^{87}Sr/^{86}Sr$ investigation of igneous apatites and carbonates using laser-ablation MC-ICPMS: Geochimica et Cosmochimica Acta, v. 67, p. 289–302, https://doi.org/10.1016/S0016-7037(02)01048-7.

Chen, F., Hegner, E., and Todt, W., 2000, Zircon ages, Nd isotopic and chemical compositions of orthogneisses from the Black Forest, Germany-evidence for a Cambrian magmatic arc: International Journal of Earth Sciences, v. 88, p. 791-802, https://doi.org/10.1007/s005310050306.

Chen, L., Liu, Y.S., Hu, Z.C., Gao, S., Zong, K.Q., and Chen, H.H., 2011, Accurate determinations of fifty-four major and trace elements in carbonate by LA-ICP-MS using normalization strategy of bulk components as 100%: Chemical Geology, v. 284, p. 283–295, https://doi.org/10.1016/j.chemgeo.2011.03.007.

Griffin, W.L., Powell, W.J., Pearson, N.J., and O'Reilly, S.Y., 2008, GLITTER: data reduction software for laser ablation ICP-MS, Laser Ablation-ICP-MS in the earth sciences: Mineralogical association of Canada short course series, v. 40, p. 204-207.

Harrison, T.M., Grove, M., McKeegan, K.D., Coath, C.D., Lovera, O.M., and LeFort, P., 1999, Origin and episodic emplacement of the Manaslu intrusive complex, central Himalaya: Journal of Petrology, v. 40, p. 3–19, https://doi.org/10.1093/petroj/40.1.3.

Hu, Z.C., Gao, S., Liu, Y.S., and Hu, S.H., 2008, Signal enhancement in laser ablation ICPMS by addition of nitrogen in the central channel gas: Journal of Analytical Atomic Spectrometry, v. 23, p. 1093–1101, https://doi.org/10.1039/b804760j.

Liu, Y.L., Williams, I.S., Chen, J.F., Wan, Y.S., and Sun, W.D., 2008, The significance of Paleoproterozoic zircon in carbonatite dikes associated with the Bayan Obo REE-Nb-Fe deposit: American Journal of Science, v. 308, p. 379–397, https://doi.org/10.2475/03.2008.08.

Ludwig, K.R., 2003, User's Manual for Isoplot 3.00, a Geochronological Toolkit for Microsoft Excel: Berkeley Geochronological Center, Special Publication, v. 4, p. 25–32.

Trotter, J.A., Williams, I.S., Barnes, C.R., Lécuyer, C., and Nicoll, R.S., 2008, Did cooling oceans trigger Ordovician biodiversification? Evidence from conodont thermometry: Science, v. 321, p. 550–554, https://doi.org/10.1126/science.1155814.

Waight, T., Baker, J., and Peate, D., 2002, Sr isotope ratio measurements by double focusing

MC-ICPMS: techniques, observations and pitfalls: International Journal of Mass Spectrometry, v. 221, p. 229–244, https://doi.org/10.1016/S1387-3806(02)01016-3.

Xie, L.W., Zhang, Y.B., Sun, J.F., and Wu, F.Y., 2008, In situ simultaneous determination of trace elements, U-Pb and Lu-Hf isotopes in zircon and baddeleyite: Chinese Science Bulletin, v. 53, p. 1565–1573, https://doi.org/10.1007/s11434-008-0086-y.

Yang, Y.H., Sun, J.F., Xie, L.W., Fan, H.R, and Wu, F.Y., 2008, In situ Nd isotopic measurement of natural geological materials by LA-MC-ICPMS: Chinese Science Bulletin, v. 53, p. 1062–1070, https://doi.org/10.1007/s11434-008-0166-z.

Yang, Y.H., Wu, F.Y., Xie, L.W., Yang, J.H., and Zhang, Y.B., 2009, In-situ Sr isotopic measurement of natural geological samples by LA-MC-ICP-MS: Acta Petrologica Sinica, v. 25, p. 3431–3441.

Yang, K.F., Fan, H.R., Santosh, M., Hu, F.F., and Wang, K.Y., 2011, Mesoproterozoic carbonatitic magmatism in the Bayan Obo deposit, Inner Mongolia, North China: Constraints for the mechanism of super accumulation of rare earth elements: Ore Geology Reviews, v. 40, p. 122–131, https://doi.org/10.1016/j.oregeorev.2011.05.008.

Yang, Y.H., Wu, F.Y., Yang, J.H., and Chew, D.M., 2014, Sr and Nd isotopic compositions of apatite reference materials used in U-Th-Pb geochronology: Chemical Geology, v. 385, p. 35–55, https://doi.org/10.1016/j.chemgeo.2014.07.012.

Data Repository File: Figure

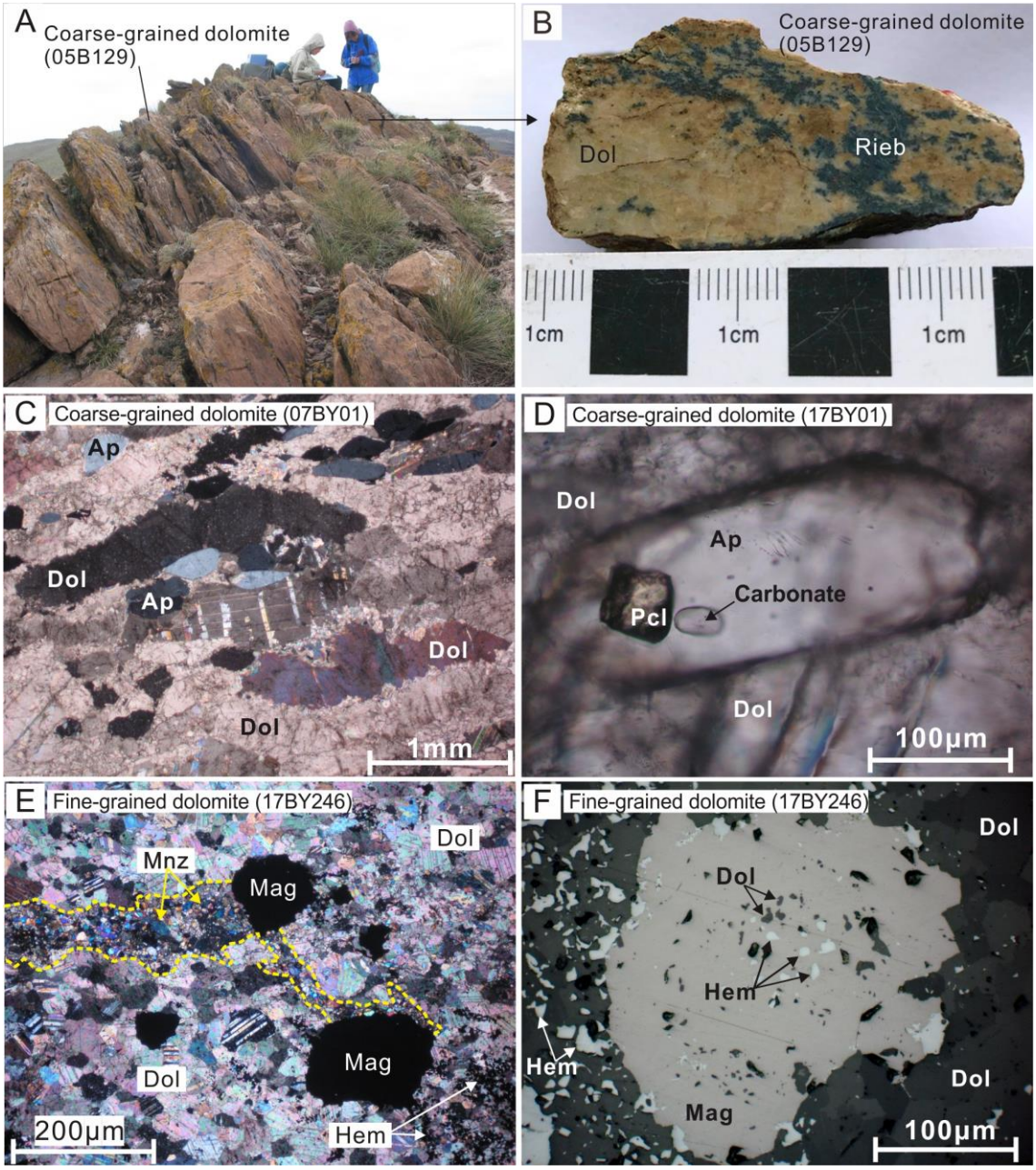

Fig. DR1. A: Outcrop of coarse-grained dolomite showing banded structure. B: Hand specimen photograph of coarse-grained dolomite with disseminated riebeckite minerals. C: Orthogonal polarized image of coarse-grained dolomite. D: Unipolarized image of apatite with pyrochlore mineral and primary carbonate inclusions from coarse-grained dolomite. E: Orthogonal polarized image of fine-grained dolomite with monazite in form of veins accompanied with magnetite. F: Reflected light image of fine-grained dolomite showing hematite and dolomite inclusions in magnetite. Abbreviations: Ap, apatite; Dol, dolomite; Hem, hematite; Mag, magnetite; Mnz, monazite; Pcl, pyrochlore; Rieb, riebeckite.

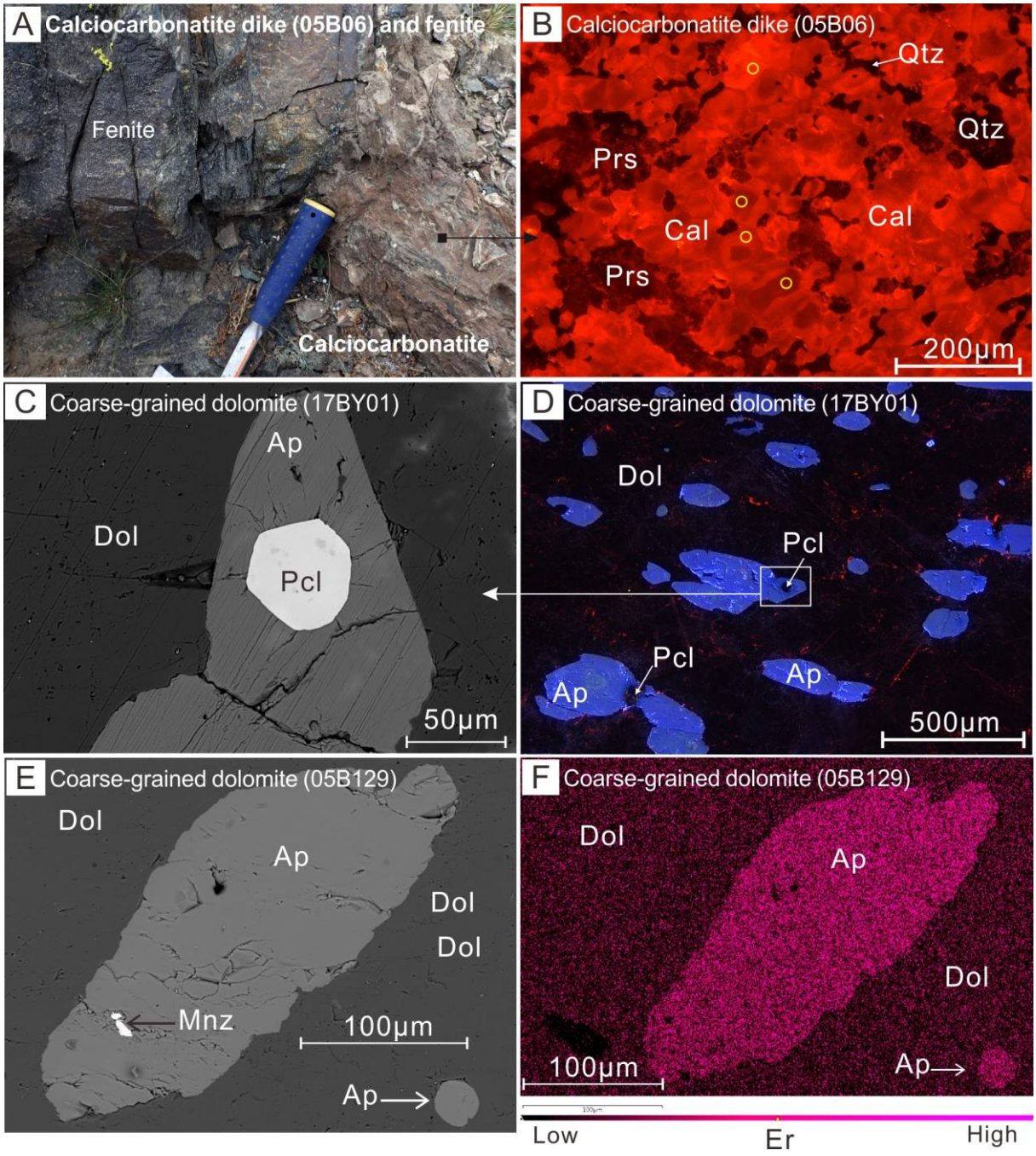

Fig. DR2. A: Outcrop of calciocarbonatite dike with intense fenitization of wall rocks. B: Cathodoluminescence (CL) images of calciocarbonatite dike with positions of *in-situ* REE analysis. C: Backscattered electron (BSE) image of apatite with pyrochlore inclusion from coarse-grained dolomite. D: CL image of coarse-grained dolomite. E: BSE image of apatite with monazite inclusion from coarse-grained dolomite. F: Energy dispersive x-ray spectroscopy (EDS) analysis of apatite from coarse-grained dolomite. Abbreviations: Ap, apatite; Cal, calcite; Dol, dolomite; Mnz, monazite; Pcl, pyrochlore; Prs, parisite; Qtz, quartz.

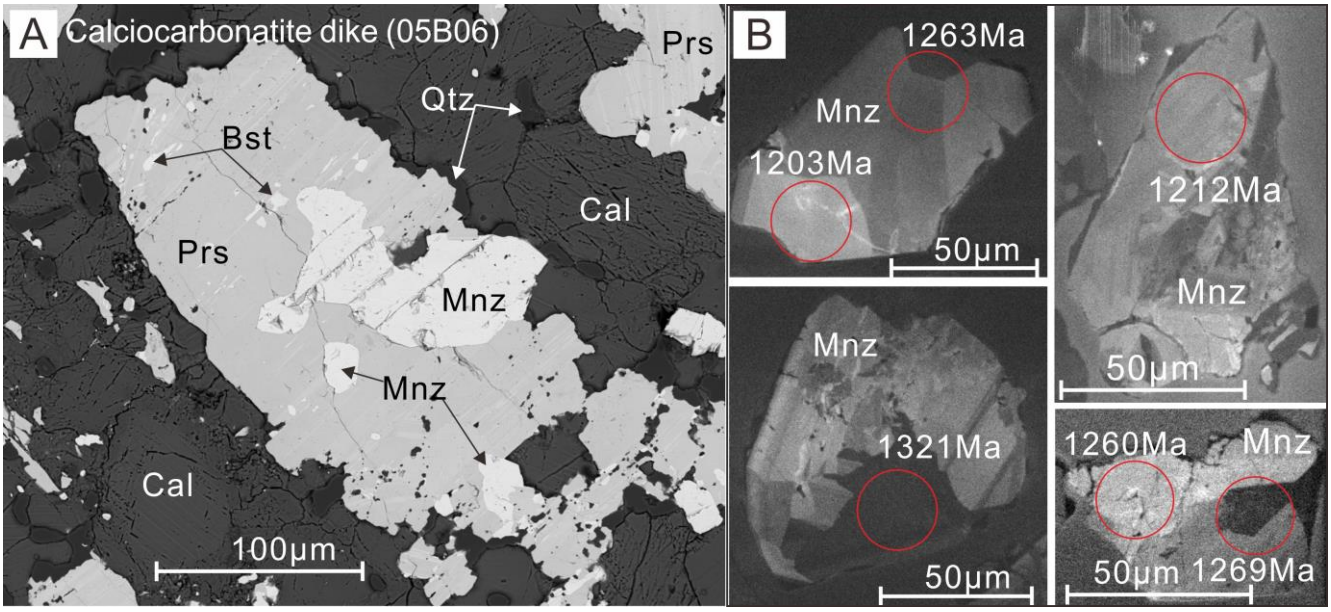

Fig. DR3. A: Backscattered electron (BSE) image of calciocarbonatite showing metasomatic relationship of monazite and parisite. B: Cathodoluminescence (CL) images of monazite in the calciocarbonatite dike showing the core and rim texture with $^{208}Pb/^{232}Th$ dating. Abbreviations: Bst, bastnaesite; Cal, calcite; Mnz, monazite; Qtz, quartz; Prs, parisite.

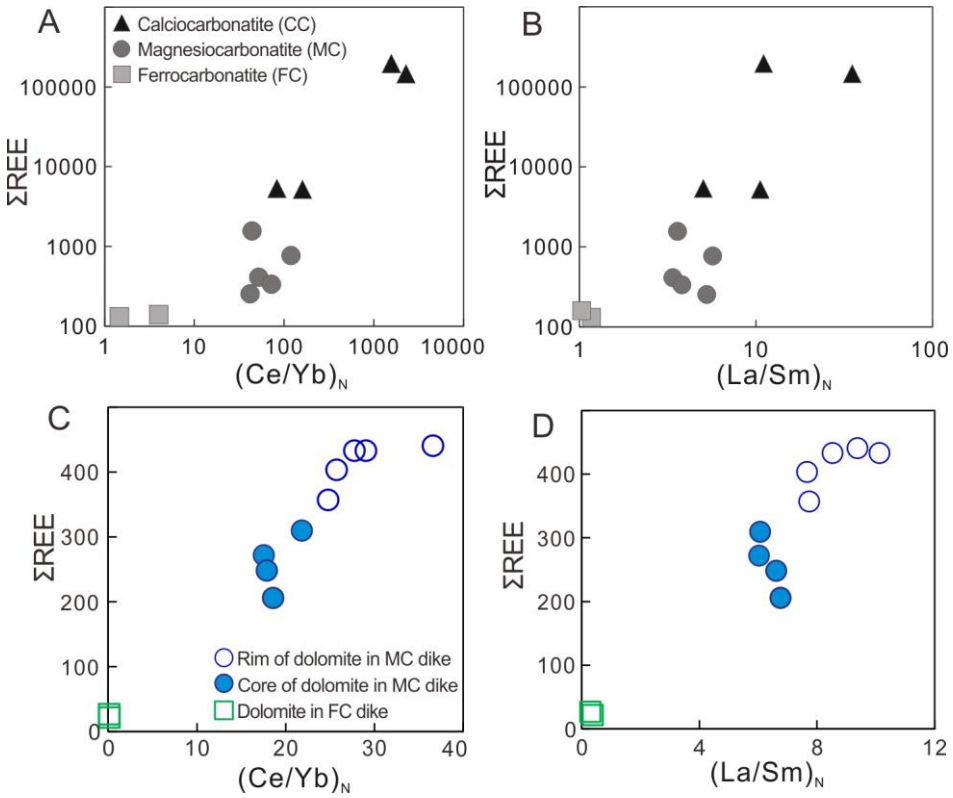

Fig. DR4. A: $(Ce/Yb)_N$ vs ∑REE diagrams of different types of carbonatite dikes. B: $(La/Sm)_N$ vs ∑REE diagrams of different types of carbonatite dikes. C: $(Ce/Yb)_N$ vs ∑REE diagrams of dolomite from ferroan and magnesian carbonatite dikes. D: $(La/Sm)_N$ vs ∑REE diagrams of dolomite from ferroan and magnesian carbonatite dikes. Whole rock data of different types of carbonatite dikes are from Yang et al., 2011.

Data Repository File: Table

Table DR1. SIMS $\delta^{18}O$ values and LA-MC-ICPMS Sr-Nd isotopes of apatite in coarse-grained dolomite (05B129, 10B10), and whole rock Sr-Nd isotopes (t = 1.3 Ga) of coarse-grained dolomite (17BY01Y), sedimentary limestone (06B272) of the Bayan Obo Group and dolomite (06B250) of the Sailinhudong Group.

Sample No.	$^{147}Sm/^{144}Nd$	2σ	$^{143}Nd/^{144}Nd$	2σ	$\varepsilon_{Nd}(t)$	Sample No.	$^{147}Sm/^{144}Nd$	2σ	$^{143}Nd/^{144}Nd$	2σ	$\varepsilon_{Nd}(t)$
05B129-01	0.0944	0.0001	0.511648	0.000046	-1.74	05B129-31	0.0967	0.0002	0.511648	0.000031	-2.14
05B129-03	0.0953	0.0001	0.511652	0.000048	-1.82	05B129-32	0.0969	0.0003	0.51166	0.000030	-1.94
05B129-04	0.1049	0.0003	0.511738	0.000037	-1.79	05B129-33	0.0957	0.0002	0.511655	0.000028	-1.83
05B129-05	0.1028	0.0006	0.511729	0.000042	-1.60	05B129-34	0.0968	0.0002	0.511671	0.000032	-1.70
05B129-06	0.0929	0.0000	0.511633	0.000028	-1.78	05B129-35	0.1010	0.0006	0.511676	0.000029	-2.33
05B129-07	0.1078	0.0005	0.511778	0.000028	-1.51	05B129-36	0.0964	0.0002	0.511640	0.000031	-2.24
05B129-08	0.0993	0.0002	0.511702	0.000024	-1.53	05B129-37	0.0941	0.0000	0.511635	0.000030	-1.94
05B129-09	0.0965	0.0002	0.511667	0.000025	-1.73	05B129-38	0.1019	0.0001	0.511717	0.000033	-1.68
05B129-10	0.0979	0.0001	0.511646	0.000031	-2.38	05B129-39	0.0972	0.0001	0.511637	0.000030	-2.44
05B129-11	0.0990	0.0002	0.511719	0.000025	-1.14	05B129-40	0.0942	0.0000	0.511645	0.000029	-1.76
05B129-12	0.0939	0.0001	0.511643	0.000026	-1.75	05B129-41	0.1077	0.0003	0.511778	0.000035	-1.49
05B129-13	0.0994	0.0012	0.511669	0.000032	-2.19	05B129-42	0.1234	0.0011	0.511878	0.000028	-2.24
05B129-14	0.1027	0.0008	0.511706	0.000028	-2.04	05B129-43	0.1028	0.0007	0.511714	0.000028	-1.90
05B129-15	0.0965	0.0001	0.511678	0.000028	-1.52	05B129-44	0.0949	0.0001	0.511685	0.000030	-1.10
05B129-16	0.1041	0.0013	0.511731	0.000029	-1.79	05B129-45	0.0943	0.0001	0.511661	0.000027	-1.47
05B129-17	0.0977	0.0004	0.511653	0.000031	-2.21	05B129-46	0.1176	0.0023	0.511823	0.000033	-2.31
05B129-18	0.0953	0.0001	0.511641	0.000030	-2.03	05B129-47	0.1010	0.0001	0.511684	0.000029	-2.17
05B129-19	0.0942	0.0004	0.511634	0.000028	-1.98	05B129-48	0.0972	0.0001	0.511664	0.000029	-1.91
05B129-20	0.0961	0.0001	0.511651	0.000028	-1.97	05B129-49	0.0943	0.0001	0.511646	0.000030	-1.76
05B129-21	0.1003	0.0002	0.511712	0.000030	-1.50	05B129-50	0.0986	0.0001	0.511688	0.000027	-1.68
05B129-22	0.0940	0.0001	0.511628	0.000027	-2.06	10B10-01	0.0998	0.0002	0.511833	0.000042	0.95
05B129-23	0.0946	0.0000	0.511617	0.000028	-2.38	10B10-02	0.1080	0.0001	0.511875	0.000029	0.36
05B129-24	0.1014	0.0002	0.511729	0.000029	-1.36	10B10-03	0.0956	0.0002	0.511712	0.000029	-0.70
05B129-25	0.0978	0.0003	0.511655	0.000049	-2.19	10B10-04	0.0981	0.0001	0.511761	0.000033	-0.17
05B129-26	0.0962	0.0002	0.511667	0.000026	-1.68	10B10-05	0.1085	0.0001	0.511902	0.000027	0.79
05B129-27	0.0968	0.0006	0.511631	0.000029	-2.49	06B250	0.1280	0.0026	0.511735	0.000034	-5.32
05B129-29	0.0966	0.0001	0.511636	0.000028	-2.35	06B272	0.1272	0.0025	0.511689	0.000036	-6.08
05B129-30	0.0960	0.0003	0.511629	0.000029	-2.39	17BY01Y	0.0894	0.0018	0.5117232	0.000014	0.30

Sample No.	$^{87}Rb/^{86}Sr$	2σ	$^{87}Sr/^{86}Sr$	2σ	$I_{Sr}(t)$
10B10-01	0.00001	0.00002	0.702679	0.000088	0.702679
10B10-02	0.00011	0.00003	0.702872	0.000076	0.702869
10B10-03	0.00001	0.00002	0.702663	0.000099	0.702663
10B10-05	0.00001	0.00002	0.702767	0.000095	0.702767
10B10-06	0.00002	0.00002	0.702767	0.000089	0.702766
10B10-07	0.00002	0.00002	0.702927	0.000097	0.702926
10B10-08	0.00003	0.00002	0.702781	0.000097	0.702780
10B10-10	0.00003	0.00001	0.702711	0.000083	0.702710
10B10-11	0.00003	0.00001	0.702776	0.000065	0.702776
10B10-12	0.00001	0.00001	0.702725	0.000069	0.702725
10B10-13	0.00002	0.00001	0.702742	0.000083	0.702741
10B10-15	0.00002	0.00001	0.702885	0.000054	0.702885
06B250	0.00471	0.00009	0.730094	0.000011	0.730000
06B272	0.07197	0.00144	0.732897	0.000011	0.731452
17BY01Y	0.00002	0.00001	0.702840	0.000072	0.702840

Sample No.	$\delta^{18}O$	2σ	Sample No.	$\delta^{18}O$	2σ
05B129-1	5.22	0.19	10B10-1	6.01	0.21
05B129-2	5.39	0.18	10B10-2	5.66	0.31
05B129-3	5.87	0.14	10B10-3	5.92	0.28
05B129-4	5.45	0.23	10B10-4	6.00	0.28
05B129-5	5.68	0.25	10B10-5	6.05	0.22
05B129-6	5.43	0.26	10B10-6	6.02	0.17
05B129-7	5.63	0.25	10B10-7	6.20	0.31
05B129-8	5.02	0.33	10B10-8	5.82	0.34
05B129-9	5.36	0.28	10B10-9	6.16	0.38
05B129-10	5.43	0.30	10B10-10	5.69	0.33

Table DR2. LA-ICPMS Th-Pb data of monazite in a calciocarbonatite dike from Bayan Obo region.

Spot No.	$^{207}Pb/^{206}Pb$	1σ(%)	$^{206}Pb/^{238}U$	1σ(%)	$^{208}Pb/^{232}Th$	1σ(%)	$^{208}Pb/^{232}Th$ (Ma)	1σ
05B06-1	1.0821	0.0734	6.6070	2.2924	0.0618	0.0008	1212.3	15.3
05B06-2	0.8620	0.0274	45.4084	28.1903	0.0561	0.0006	1103.7	12.1
05B06-3	0.9686	0.0285	4.2051	0.3349	0.0379	0.0004	751.2	8.2
05B06-4	0.9463	0.0516	16.2956	9.6263	0.0489	0.0006	964.8	11.2
05B06-5	0.7988	0.0280	0.5434	0.0233	0.0205	0.0003	410.5	6.2
05B06-6	0.9216	0.0151	23.4420	2.5050	0.0469	0.0005	926.9	10.0
05B06-7	0.8999	0.0180	10.9744	1.0244	0.0542	0.0006	1066.0	11.5
05B06-8	0.9449	0.0122	70.1310	7.9705	0.0525	0.0006	1034.7	11.2
05B06-9	0.8439	0.0239	8.5642	1.0604	0.0530	0.0006	1043.1	11.3
05B06-10	0.9146	0.0159	12.8635	1.0753	0.0629	0.0008	1232.9	14.3
05B06-11	1.0366	0.0517	16.5723	6.7966	0.0559	0.0007	1098.6	12.6
05B06-12	0.9431	0.0136	15.4001	1.1125	0.0393	0.0004	778.9	8.3
05B06-13	0.9125	0.0227	20.1566	3.5591	0.0595	0.0007	1168.8	13.2
05B06-15	0.6169	0.0258	0.4720	0.0219	0.0480	0.0005	948.5	10.2
05B06-16	1.0477	0.0990	8.6781	5.9433	0.0592	0.0007	1162.6	12.8
05B06-17	1.2833	1.1856	0.3805	0.3464	0.0570	0.0007	1120.8	12.6
05B06-18	0.9164	0.0489	11.9386	4.0046	0.0485	0.0006	957.3	10.6
05B06-19	0.9142	0.0194	12.2301	1.1743	0.0518	0.0006	1021.5	10.8
05B06-20	0.8295	0.0421	1.3304	0.0983	0.0249	0.0003	496.8	6.3
05B06-21	0.8328	0.0315	6.8459	1.1475	0.0577	0.0006	1134.0	12.2
05B06-22	0.9214	0.0128	12.3828	0.6783	0.0643	0.0008	1260.3	14.5
05B06-23	0.9233	0.0198	10.4570	0.9697	0.0430	0.0005	851.3	9.6
05B06-24	1.0643	0.0197	10.0771	0.7585	0.0648	0.0008	1268.9	14.6
05B06-25	0.8187	0.0426	2.3859	0.2538	0.0576	0.0006	1131.9	12.3
05B06-26	0.4482	0.1241	4.1503	2.6422	0.0583	0.0006	1145.9	12.3
05B06-27	0.8015	0.0499	30.0882	36.5798	0.0572	0.0006	1124.1	12.0
05B06-28	0.5166	0.1661	1.4100	0.5525	0.0567	0.0006	1115.1	11.8
05B06-29	0.9105	0.0677	10.2866	4.9961	0.0578	0.0007	1134.8	13.0
05B06-30	0.9891	0.0512	21.3902	13.7922	0.0558	0.0006	1097.5	11.6
05B06-32	1.0656	0.0142	26.3887	2.1830	0.0675	0.0008	1320.6	14.2
05B06-34	1.2655	0.1030	44.3225	22.9918	0.0613	0.0008	1203.2	15.7
05B06-35	0.9139	0.0425	11.4705	3.0051	0.0645	0.0008	1262.8	14.9

Table DR3. LA-ICPMS REE and trace elements (ppm) of calcite in calciocarbonatite dikes, dolomite in magnesiocarbonatite and ferrocarbonatite dikes, dolomite and apatite in coarse-grained dolomite from Bayan Obo region with whole rock REE and trace elements (ppm) of coarse-grained dolomite for comparison.

Mineral /rock	Apatite in coarse-grained dolomite																			
Sample No.	17BY01										05B129					10B10				
Rb	0.02	0.02	0.03	0.02	0.04	0.02	0.03	0.03	0.02	0.02	0.02	0.06	0.12	0.01	0.03	0.05	0.01	0.02	0.04	0.08
Ba	56.84	38.09	75.96	56.56	47.86	52.45	71.25	89.95	59.19	46.89	44.40	34.40	38.20	41.80	46.50	35.40	33.40	50.90	123.0	33.40
Th	23.13	2.96	23.02	7.27	23.75	4.96	32.60	6.08	18.60	36.23	6.96	8.47	5.65	8.02	15.80	1.56	5.26	7.35	9.66	14.84
U	0.00	0.00	0.00	0.00	0.00	0.00	0.00	0.00	0.00	0.00	0.00	0.01	0.02	0.00	0.01	0.02	0.00	0.00	0.00	0.00
Pb	7.90	5.40	8.19	7.85	7.28	8.63	8.97	7.83	9.13	8.48	4.28	4.20	2.88	4.65	5.79	3.55	3.77	4.87	4.42	4.79
Nb	0.06	0.02	0.13	0.11	0.02	0.02	0.11	0.14	0.06	0.02	0.08	0.05	0.11	0.06	0.05	0.03	0.06	0.10	0.20	0.02
Ta	0.00	0.00	0.00	0.00	0.00	0.00	0.00	0.00	0.00	0.00	0.00	0.00	0.00	0.00	0.00	0.01	0.01	0.00	0.01	0.00
La	1584	1065	1611	1741	1514	1697	1822	1523	1555	1797	1203	991.0	865.0	1103	1628	581.0	594.0	1000	1235	816.0
Ce	3736	2627	3783	4079	3640	4114	4187	3525	3619	4180	2931	2721	2181	3106	3900	1998	1834	2415	2985	2894
Pr	457.4	325.6	458.9	490.2	444.4	505.3	503.9	421.8	439.8	505.4	365.0	377.0	281.0	421.0	476.0	290.0	260.0	300.0	371.0	438.0
Sr	9980	10288	10661	10716	9534	10147	9751	10322	10263	9758	8464	8928	7922	8073	8833	16712	14176	9533	11280	11699
Nd	1883	1343	1893	1966	1851	2051	2042	1698	1798	2074	1413	1598	1120	1734	1830	1200	1106	1155	1483	1984
Zr	0.04	0.04	0.04	0.09	0.02	0.03	0.03	0.05	0.05	0.03	0.14	0.01	0.14	0.05	0.05	0.00	0.00	0.20	0.17	0.00
Hf	0.00	0.00	0.00	0.00	0.00	0.01	0.01	0.00	0.00	0.00	0.01	0.00	0.02	0.02	0.01	0.00	0.00	0.01	0.00	0.03
Sm	291.8	208.4	293.5	275.9	294.9	301.0	317.3	250.0	286.8	319.3	226.0	292.0	171.0	306.0	286.0	242.0	219.0	177.0	238.0	381.0
Eu	80.77	56.64	80.35	71.56	81.94	79.41	87.02	65.96	78.84	88.13	58.00	81.90	45.40	82.70	74.70	68.10	61.60	45.50	62.90	104.0
Gd	192.8	135.9	192.9	166.1	194.6	185.4	206.4	155.6	189.1	210.7	152.0	222.0	115.0	226.0	197.0	185.0	160.0	114.0	166.0	274.0
Tb	20.22	13.79	20.12	16.59	20.27	19.01	21.93	15.74	19.89	21.97	14.40	21.70	11.00	22.40	19.30	19.40	17.50	11.30	15.50	25.60
Dy	88.51	58.63	87.94	70.01	88.55	80.90	95.95	66.92	86.53	96.44	66.10	104.00	49.80	104.00	90.40	92.20	84.50	48.80	70.00	118.00
Y	277.7	176.5	280.4	210.4	285.9	253.8	308.2	207.0	284.4	307.3	228.0	351.0	162.0	349.0	317.0	322.0	306.0	149.0	219.0	392.0
Ho	12.45	8.10	12.55	9.54	12.53	11.20	13.47	9.19	12.34	13.57	10.10	16.00	7.52	15.50	14.10	14.40	13.40	6.76	9.96	17.70
Er	23.77	14.73	23.75	17.58	24.05	20.93	25.98	17.28	22.95	25.73	21.20	31.90	15.20	32.00	28.90	30.00	28.50	13.00	19.10	36.60
Tm	2.25	1.42	2.26	1.71	2.27	2.03	2.54	1.70	2.16	2.55	1.87	3.05	1.60	2.86	2.79	2.73	2.69	1.16	1.96	3.16
Yb	10.62	6.53	10.60	8.05	10.50	9.58	11.60	8.13	9.98	11.36	9.30	13.70	6.39	11.90	13.00	11.80	13.90	5.83	7.78	13.40
Lu	1.07	0.68	1.09	0.84	1.09	1.01	1.24	0.85	1.04	1.20	1.13	1.51	0.77	1.56	1.58	1.37	1.63	0.64	0.76	1.40
∑REE	8385	5865	8471	8914	8180	9078	9338	7758	8122	9348	6473	6473	4871	7169	8562	4737	4398	5293	6666	7106
$(La/Yb)_N$	107.0	116.9	109.1	155.2	103.4	127.0	112.7	134.3	111.8	113.4	92.90	52.00	97.10	66.70	89.60	35.30	30.70	123.0	113.8	43.60
Eu*	1.04	1.03	1.03	1.02	1.05	1.03	1.04	1.02	1.04	1.04	0.96	0.98	0.99	0.96	0.96	0.98	1.01	0.98	0.97	0.98

Table DR3 continued.

Mineral /rock	Calcite in calciocarbonatite dyke											
Spot position	Rim					Core						
Sample No.	05B06-R					05B06-C						
Rb	0.03	0.01	0.00	0.01	0.02	0.02	0.01	0.02	0.00	0.03	0.02	0.02
Ba	317.3	289.8	226.2	274.8	265.3	228.8	281.9	209.8	283.5	504.5	355.5	314.3
Th	0.01	25.54	0.01	1.27	0.71	0.00	0.81	0.04	0.41	2.48	0.61	2.95
U	0.00	0.26	0.00	0.01	0.02	0.00	0.00	0.00	0.00	0.09	0.01	0.04
Pb	17.84	18.45	16.70	18.50	18.50	18.65	17.48	17.98	18.74	26.93	19.11	20.01
Nb	0.00	0.00	0.00	0.09	0.05	0.00	0.01	0.00	0.00	0.01	0.01	0.00
Ta	0.00	0.00	0.00	0.00	0.00	0.00	0.00	0.00	0.00	0.00	0.00	0.00
La	43.20	72.24	42.81	106.94	42.31	35.61	44.06	23.08	56.09	46.12	33.45	20.24
Ce	113.3	143.7	109.2	188.4	107.8	89.38	109.2	55.48	89.82	101.8	88.52	62.61
Pr	14.00	16.31	13.37	19.84	13.36	10.45	13.00	6.47	12.52	12.31	10.93	8.13
Sr	14517	15288	17027	13214	13779	14187	12959	10886	13181	14035	13063	12537
Nd	56.99	62.04	52.92	71.72	54.84	41.14	50.68	25.39	48.10	48.28	46.24	35.30
Zr	0.57	0.06	0.09	0.15	0.01	0.00	0.34	0.01	0.03	1.07	0.00	0.23
Hf	0.01	0.00	0.01	0.02	0.00	0.00	0.02	0.00	0.00	0.13	0.00	0.00
Sm	12.80	12.41	12.01	14.57	11.79	8.07	10.70	5.99	9.74	10.51	10.32	8.41
Eu	4.99	4.78	4.77	5.17	4.36	3.23	4.28	2.54	3.78	4.25	4.19	3.35
Gd	11.81	11.25	10.02	12.59	10.48	7.26	10.52	6.75	9.21	9.23	10.11	8.10
Tb	2.15	2.02	1.66	2.05	1.75	1.28	1.93	1.37	1.78	1.81	1.87	1.59
Dy	13.90	13.05	10.97	13.12	10.40	9.56	12.35	10.50	12.14	11.98	12.11	10.49
Y	72.44	67.21	59.44	68.03	54.02	55.11	68.97	63.93	66.44	65.84	63.96	59.13
Ho	2.80	2.64	2.19	2.69	2.09	2.18	2.94	2.55	2.73	2.62	2.53	2.45
Er	7.69	7.09	6.40	7.21	5.74	6.93	8.61	8.05	8.46	7.29	7.41	7.61
Tm	1.07	1.10	1.01	1.07	0.90	1.23	1.37	1.36	1.27	1.13	1.23	1.26
Yb	7.49	7.19	6.70	7.14	6.28	8.86	10.09	9.36	9.44	7.98	8.52	9.61
Lu	1.17	1.09	0.86	1.00	0.98	1.32	1.62	1.32	1.42	1.16	1.38	1.59
∑REE	293.4	356.9	274.9	453.5	273.1	226.5	281.3	160.2	266.5	266.5	238.8	180.8
$(La/Yb)_N$	4.14	7.21	4.58	10.74	4.83	2.88	3.13	1.77	4.26	4.14	2.82	1.51
Eu*	1.24	1.24	1.33	1.17	1.20	1.29	1.23	1.22	1.22	1.32	1.25	1.24
MgO	0.18	0.18	0.20	0.18	0.18	0.18	0.19	0.19	0.19	0.19	0.20	0.21
CaO	52.81	52.90	52.49	51.50	52.90	52.82	53.00	53.06	52.96	52.77	52.80	52.90
MnO	1.11	1.09	1.10	0.99	1.20	1.15	1.14	1.25	1.12	1.11	1.16	1.20
$Fe_2O_3^T$	0.50	0.49	0.49	0.50	0.52	0.52	0.57	0.65	0.57	0.58	0.56	0.61

Table DR3 continued.

Mineral /rock	Dolomite in magnesiocarbonatite dyke									Dolomite in ferrocarbonatite dyke		Dolomite in corese-grained dolomite		Whole rock Coarse-grained dolomite
Spot position	Rim					Core								
Sample No.	M3-2-R					M3-2-C				M12-2-D		17BY01		
Rb	0.00	0.00	0.02	0.05	0.00	0.00	0.05	0.01	0.00	0.27	0.06	0.02	0.01	0.20
Ba	652.6	657.7	686.0	646.5	579.0	625.5	540.1	599.4	640.5	32.37	21.27	76.62	86.13	86.50
Th	0.01	0.01	0.00	0.02	0.01	0.01	0.01	0.01	0.00	0.05	0.04	0.01	0.00	4.08
U	0.41	0.00	0.00	0.01	0.00	0.00	0.00	0.00	0.00	0.00	0.00	0.01	0.00	0.41
Pb	15.19	14.97	14.80	15.33	13.90	16.32	18.51	16.11	17.04	1.26	1.84	44.27	47.74	83.21.
Nb	0.00	0.00	0.01	0.00	0.00	0.00	0.00	0.00	0.00	0.18	0.08	0.24	0.00	402.0
Ta	0.00	0.00	0.00	0.00	0.00	0.00	0.00	0.00	0.00	0.00	0.00	0.00	0.00	0.80
La	93.40	116.9	118.2	105.4	119.6	66.00	73.62	51.80	60.67	0.65	0.71	11.59	20.49	60.70
Ce	166.02	201.9	202.8	187.6	204.3	124.3	144.7	93.39	113.4	2.73	2.05	25.48	45.89	149.0
Pr	16.54	20.27	20.35	18.79	21.05	12.77	15.30	9.90	11.70	0.45	0.33	2.77	5.01	17.45
Sr	9280	9226	9357	9267	9144	9307	8818	9012	9187	2524	4159	4557	4855	5040
Nd	57.29	67.81	68.03	64.63	72.11	46.27	52.43	34.25	41.95	2.45	1.91	10.18	18.54	67.80
Zr	0.00	0.03	0.01	0.00	0.02	0.02	0.02	0.00	0.01	0.13	0.05	0.00	0.02	4.00
Hf	0.00	0.01	0.00	0.00	0.00	0.00	0.00	0.00	0.00	0.00	0.00	0.00	0.00	0.20
Sm	7.79	8.84	7.53	8.87	8.23	7.05	7.83	4.94	5.91	1.38	1.18	1.61	2.90	10.25
Eu	1.76	1.96	1.94	2.04	2.05	1.64	1.74	1.35	1.51	0.61	0.63	0.48	0.83	2.77
Gd	4.99	5.63	4.97	5.50	5.03	4.26	4.34	3.42	4.27	2.02	1.97	1.10	2.00	7.22
Tb	0.71	0.72	0.67	0.73	0.64	0.65	0.70	0.49	0.60	0.41	0.45	0.14	0.26	0.78
Dy	3.65	3.83	3.62	4.42	3.35	3.64	3.72	2.55	3.60	3.41	3.63	0.68	1.27	3.41
Y	19.15	20.04	18.78	21.21	16.38	20.21	19.78	14.16	18.62	25.41	22.90	2.83	5.61	11.90
Ho	0.75	0.72	0.68	0.80	0.64	0.74	0.76	0.54	0.70	0.92	0.86	0.12	0.22	0.50
Er	1.85	1.95	1.74	2.00	1.65	2.04	2.04	1.45	1.76	3.51	2.94	0.30	0.53	1.08
Tm	0.26	0.28	0.24	0.30	0.27	0.27	0.31	0.24	0.27	0.77	0.47	0.03	0.07	0.12
Yb	1.86	2.02	1.94	2.02	1.55	1.97	1.84	1.40	1.76	6.43	3.95	0.22	0.52	0.57
Lu	0.26	0.29	0.28	0.31	0.24	0.30	0.27	0.19	0.27	1.16	0.64	0.03	0.09	0.07
∑REE	357.1	433.1	433.0	403.5	440.7	271.9	309.6	205.9	248.4	26.9	21.7	54.7	98.6	321.7
$(La/Yb)_N$	36.02	41.50	43.68	37.35	55.30	24.04	28.68	26.60	24.68	0.07	0.13	37.02	28.47	76.39
Eu*	0.86	0.85	0.97	0.89	0.98	0.91	0.91	1.00	0.92	1.11	1.26	1.11	1.05	0.98
MgO	17.93	18.11	17.96	17.92	18.21	17.84	17.73	17.80	17.87	13.34	13.33	18.50	18.40	18.55
CaO	30.95	30.84	30.97	31.04	30.64	30.75	30.75	30.81	30.66	29.26	29.15	30.59	30.52	30.20
MnO	1.12	1.11	1.12	1.09	1.09	1.11	1.11	1.11	1.13	2.85	3.07	0.58	0.64	0.61
$Fe_2O_3^T$	2.38	2.43	2.39	2.40	2.44	2.77	3.06	2.71	2.85	10.18	9.75	3.30	3.50	3.65